

## **Simultaneous observations of the cusp with IMAGE Low Energy Neutral Atoms Imager and SuperDARN radar**

S. Taguchi,<sup>1</sup> K. Hosokawa,<sup>1</sup> M. R. Collier,<sup>2</sup> T. E. Moore,<sup>2</sup> M.-C. Fok,<sup>2</sup>  
A. S. Yukimatu,<sup>3</sup> N. Sato,<sup>3</sup> and R. A. Greenwald<sup>4</sup>

<sup>1</sup> Department of Information and Communication Engineering, University of Electro-Communications, Chofu, Tokyo, 182-8585

<sup>2</sup> NASA Goddard Space Flight Center, Greenbelt, MD 20771, USA

<sup>3</sup> National Institute of Polar Research, Itabashi, Tokyo, 173-8515

<sup>4</sup> Applied Physics Laboratory, The Johns Hopkins University, Laurel, MD 20723, USA

Correspondence to: taguchi@ice.uec.ac.jp

Running Title: IMAGE/LENA and SuperDARN Observations of the Cusp

Key words: Polar cusp, magnetopause, magnetosheath, neutral atoms, and HF radars

Advances in Polar Upper Atmosphere Research, in press

**Abstract.**

The Low Energy Neutral Atom (LENA) imager on the IMAGE spacecraft observed significant emission in the high-latitude magnetosheath direction during an extreme solar wind condition on April 11, 2001. The emission was modulated in such a manner that the sources shifted equatorward in the high-latitude sheath while sometimes undergoing brief poleward returns. This modulation and the IMF  $B_z$  tend to have correlative variations. During this interval of interest, SuperDARN was receiving strong backscattered signals from large portions of the dayside ionosphere. This observation indicates that the equatorward motion of the cusp latitude consists of rapid and slow phases. This kind of equatorward shift appears to correlate with the motion of the emission observed by LENA in the direction of the high-latitude sheath, which gives evidence for a means for monitoring the high-altitude cusp using IMAGE/LENA. It thus appears that the two remote sensing observations, i.e., IMAGE/LENA and SuperDARN radar would provide promising opportunities to understand the detailed dynamics of the polar cusp extending from the low-altitudes to the high-altitudes.

**1. Introduction**

Many authors have examined the effect of the solar wind on the polar cusp at low altitudes, using plasma observations from spacecraft [e.g., Burch et al., 1973; Meng, 1983; Newell and Meng, 1989], from observations of auroral emission using optical ground-based techniques [e.g., Sandholt et al., 1994, 1998], and from measurements of ionospheric plasma convection with coherent HF radars [e.g., Greenwald, 1990; Pinnock, 1993]. The space-based optical imaging has also contributed to our understanding of the low-altitude cusp [Milan et al., 2000; Fuselier et al., 2002; Frey et al., 2002], and the characteristics of the low-altitude cusp are now well understood.

For the understanding of the solar wind control on the mid- and high-altitude polar cusp, the POLAR spacecraft and the Hawkeye spacecraft have made a significant contribution. Using the POLAR data, Zhou et al. [2000] identified a large number of polar cusp crossings, and modeled the position of the high-altitude cusp including its dependence on the solar wind conditions. At higher altitudes than POLAR Hawkeye spacecraft, which can traverse at altitudes greater than  $10 R_E$ , has also revealed well-defined cusp crossings [e.g., Farrell and Van Allen 1990]. The typical duration of these cusp crossings seems to be ~30 min to ~1 hour.

While such long-duration cusp observations can provide detailed information on the structure inside the cusp, they would exceed the several-minute response time of the high-altitude cusp to rapid solar wind variations. In other words, results from analyses of the well-defined interval of the cusp crossing at such high altitudes reflect the cusp response to

the solar wind for a timescale longer than  $\sim 30$  min. In order to understand the shorter time-scale response, the field and plasma variations embedded in the large-scale structure must be investigated as far as in-situ spacecraft observations are concerned. Chen et al. [1997] showed a Hawkeye event identified in a possible location of the cusp indentation, and associated the observed plasma and magnetic field variations, which had a time scale of several minutes, with the motion of the cusp as modulated by the varying IMF. Although collection of this kind of event from in situ observations actually gives insights into our understanding of the dynamics of the high-altitude cusp, in using a single spacecraft it is difficult to find many cusp-crossing events that can be correlated with IMF variations with a time scale of several minutes.

Remote sensing studies with the low energy neutral atom (LENA) imager [Moore et al., 2000] on the IMAGE spacecraft have recently shown that neutral particles detected by LENA in the magnetosphere include the result of solar-wind ions charge-exchanging with the hydrogen exosphere in the magnetosheath flow [Collier et al., 2001ab, Fok et al., 2003, Moore et al., 2003]. Extending their finding, Taguchi et al. [2003] have shown that the LENA emissions observed in the direction of the high-latitude magnetosheath reflect the cusp indentation in the magnetopause shape, which suggests a means for monitoring the cusp motion using LENA. In this paper, using simultaneous observations at different altitudes with IMAGE and SuperDARN radar on April 11, 2001, we show that the motion of the emission observed by LENA at high-altitudes and the latitudinal motion of the backscatter signal detected by SuperDARN in the dayside ionosphere has similar variations, which supports the above suggestion, i.e., the capability of the IMAGE/LENA to monitor the high-altitude cusp.

## 2. Solar Wind Conditions on April 11, 2001

Figure 1 shows solar wind conditions for the event that we analyzed in this study. The top six panels are solar wind data obtained at the ACE spacecraft located about  $220 R_E$  upstream of the Earth. Panel (a) shows that solar wind ions with energies between 47 and 65 keV/e (obtained by the ACE Electron, Proton, and Alpha Monitor), which includes the 50 keV/e low limit for LENA ion admittance, have a very steady flux. This suggests that if the energetic ions penetrating the collimator cause LENA variation, it would be a relatively constant effect. In other words, if the LENA response varies, it strongly suggests that the LENA response is not due to the energetic ions [Collier et al., 2001a].

Panels (b) and (c) of the Figure show respectively the IMF  $B_Y$  and  $B_Z$  in GSM coordinates.  $B_Z$  reaches a very large negative value, i.e.,  $< -35$  nT around 1543 UT. We plotted 64-s averages of IMF data that were created from original 16-s averages so as to make comparison between the IMF and plasma data easier. The RAM pressure in Panel (f)

of the Figure was calculated from the density (panel (d)) and speed (panel (e)) assuming 4%  $\text{He}^{++}$  particles.

Panel (g) shows the H-component of the SYM index [Iyemori and Rao, 1996]. Two clear sudden impulses ( $\text{SI}^+$ ) can be seen at the times shown with the vertical lines in Panel (g). As the start of the larger  $\text{SI}^+$  we took 1548 UT (right line), i.e., the first increase of more than 5 nT/min. At 1528 UT ACE observed a sharp increase in the solar wind dynamic pressure. The time lag from ACE to the Earth is then estimated to be 20 ( $= 1548 - 1528$  UT) min. A similar time lag can be obtained for another  $\text{SI}^+$  at 1519 UT (Panel (g)) if we relate this  $\text{SI}^+$  to the RAM pressure jump at 1459 UT (left line in Panels (d) to (f)), which is the largest jump before the major jump. The 20 min time lag is shorter than the simple solar wind convection time  $\sim 36$  min, which is calculated from the ACE  $X$  location of  $220 R_E$  and solar wind speed of  $\sim 650$  km/s. However, such a difference is not surprising when we consider that large timing uncertainties exist in estimating the solar wind convection [Collier et al., 1998]. The shorter lag is reasonable when we assume that the phase fronts are along the magnetic field. ACE is located at negative  $Y$  ( $= -9 R_E$ ) and the IMF has positive  $B_X$  and negative  $B_Y$  components (not shown).

### 3. Sheath Emission observed by IMAGE/LENA

Figure 2 shows the IMAGE orbit in the  $X_{\text{GSM}}\text{-}Z_{\text{GSM}}$  plane during the period 1540 – 1620 UT on April 11, 2001. IMAGE is located near  $(X_{\text{GSM}}, Z_{\text{GSM}}) \sim (4 R_E, 4 R_E)$  in the mid-noon sector ( $Y_{\text{GSM}} \sim -0.2 R_E$ , not shown). For this kind of mid-noon orbits, the spin angles ( $0^\circ$  to  $360^\circ$ ) of LENA can take a whole image in the  $X_{\text{GSM}}\text{-}Z_{\text{GSM}}$  meridian. During the above period, the solar direction corresponds to the spin angle of  $\sim 130^\circ$ , and the angle of  $\sim 220^\circ$  ( $= 130^\circ + 90^\circ$ ) looks roughly in the direction parallel to the positive  $Z_{\text{GSM}}$ .

Figure 3 shows the variations of the IMAGE  $Z_{\text{GSM}}$  position, the LENA spin angle ranges we used in our analysis, the LENA hydrogen total count rates, the normalized count profile versus spin angles, and the distance representing the direction for the maximum count peaks. In Panel (b), the spin angle sector that includes the Sun signal, which we have not focused on in this study, occurs between the two gray regions. The details of the cause of the Sun signal, including its long-term variations, have been reported by Collier et al. [2003, 2001a and b]. IMAGE was located at positive  $Z_{\text{GSM}}$ , as shown in Figure 2 and Panel (a) of Figure 3, and the spin angle range lower than the solar direction represents line of sight (LOS) that can intersect the equatorial plane. This lower angle range (lower shaded region in Panel (b)) for each time was determined as angles for which such intersection occurs between the radial distances of  $4.5 R_E$  and of  $12 R_E$ , considering the possible subsolar distance of the magnetopause. For the higher shaded part, the lower boundary ( $157^\circ$ -bin) was taken as the sector that is three sectors ( $= 24^\circ$ ) from the position of the Sun

signal. The upper boundary was decided as a sector bin whose LOS makes the minimum angle from the  $Z$ -axis.

Panel (c) shows the total counts from the two gray regions. Three enhancements are identified around 1553, 1557, and 1603 UT (dashed lines). Panel (d) shows a spectrogram of the two gray regions in Panel (b). Counts are normalized so that the maximum peak of the hydrogen background adjusted rate can be unity in each time and range. Blanks at 1609 and 1613 UT in the upper range mean that no emission is identified. In the upper range, emission peaks (red regions) shift to smaller angles in coincidence with the total count enhancements (in Panel (c)), which suggests that the source shifts equatorward at the enhancements. This kind of characteristic can be more clearly identified for the locations of the peak count on a reference sphere (Panel (e)).

We used a sphere of the radial distance of  $6.6 R_E$  as a reference sphere because during this observation GOES 8 actually observed multiple magnetopause crossings on the dayside in geosynchronous orbits (not shown). Panel (e) represents how distant the intersection of the LOS of the peak count, i.e., the red dot (in Panel (d)) is from the equatorial plane as measured on this reference sphere. The definition of this distance,  $D$ , is illustrated in inset (Panel (e)). We focus on  $D$  at high spin angles in this paper. For the emission at low spin angles, i.e., the emission in the direction of the low-latitude sheath, Taguchi et al. [2003] have clarified its characteristics in connection with the compressed magnetopause observed by GOES 8.

In the upper range,  $D$  tends to decrease while undergoing brief increases at three times. Taguchi et al. [2003] have suggested that the high-latitude emission represents the cusp indentation in the magnetopause shape. If this is correct, the variation of  $D$  in the upper range (Panel (e) of Figure 3) implies that the cusp moves equatorward while undergoing brief poleward shifts. We will compare this kind of variations with the SuperDARN radar backscattered signals from the dayside ionosphere near the cusp.

Two examples of the LENA high-latitude snapshot signals are shown in Figure 4. The background-adjusted hydrogen count rates for a 2 min interval starting at 1549:20 UT and those for an interval from 1601:47 UT are plotted in the format of spin angle versus polar angle in Figures 4a and 4b, respectively. It is clear that the emission in Figure 4b occurs at lower spin angles than that in Figure 4a.

#### 4. Simultaneous Observations With SuperDARN and IMAGE/LENA

During the interval of interest SuperDARN Goose Bay and Kapuskasing radars were located in the daytime sector. Around 1550 UT the radar at Goose Bay was located near mid-noon, and receiving strong backscattered signals from the dayside ionosphere. We analyzed data from the normal global scan. The time resolution of the data is approximately 90s.

Figure 5 shows a combined plot of the flow velocity along the LOS for Beam 5 and the value of  $D$  for the LENA high-latitude sheath emission, together with ACE solar wind. In Panels (a) and (b) of Figure 5, the ACE data are delayed by 20 min. The Alfvénic propagation of information from the magnetosphere to the ionosphere is thought to be about 2 min [e.g., Ruohoniemi et al., 1993; Khan and Cowley 1999]. SuperDARN data in Panel (c) are forwarded by 2.5 min, and superimposed on the variations of  $D$  in an arbitrary scale along the vertical axis. The calculation of the magnetic latitude for the vertical axis of the radar signal plot is based on the Altitude Adjusted Corrected Geomagnetic Coordinate system [Baker and Wing, 1989]. Around 1545 UT the equatorward boundary of the fast anti-sunward flow region (the reddish color) was  $\sim 76^\circ$  in magnetic latitude. Then, the boundary moved equatorward, and reached around  $67^\circ$  after 1600 UT.

The value of  $D$  tends to decrease while undergoing a brief poleward return three times. Similar variations can be also seen in IMF  $B_Z$ . Considering that  $B_Z$  is a controlling parameter for the cusp location, the existence of a close relation between  $B_Z$  and  $D$  shows that  $D$  reflects the cusp location. This supports that the recent suggestion that the high-latitude emission observed by LENA represents the cusp indentation [Taguchi et al., 2003]. This correlation depends on the 20 min delay time of the ACE data, which comes from the comparison between the solar wind dynamic pressure and  $SI^+$  in the geomagnetic index, as was discussed in Figure 1. Since the LENA data are obtained in the magnetosphere, the 20 min delay, which is based on the geomagnetic index, might include error. However, the choice of 20 min seems to be reasonable. The reason will be briefly discussed later.

The motion of the equatorward boundary of the signals appears to consist of rapid and slow stages. The numbers 1, 2, and 3 in Panel (c) of Figure 4 indicate the time for the rapid equatorward shift of the radar signals. This timing is also indicated in the IMF  $B_Z$  data (Panel (b)) with the purple lines. It is evident that the time of each purple line corresponds to the large, negative  $B_Z$ .

The rapid equatorward shift of the radar signals at the time of Numbers 1 to 3 in Panel (c) of Figure 5 also corresponds to the equatorward shift of  $D$ . Immediately after this kind of equatorward shifts,  $D$  undergoes a brief poleward return, and this change is in coincident with the very slow phase of the equatorward boundary of the radar signals although the situation is somewhat hard to see after the time of Number 3.

HF radars are particularly sensitive to cusp region backscatter [Milan et al., 1998]. The equatorward edge of the backscatter showing the broad Doppler spectral widths coincides with the equatorward edge of the cusp particle precipitation region [Baker et al., 1990; Yeoman et al. 1997; Hosokawa et al., 2002]. As would be expected, the equatorward portion of the backscatter signals during the interval in Figure 5 has broad spectral widths (not shown). The radar appears to be monitoring the cusp region. The correlation of the latitude of the radar signals with the negative  $B_Z$  of IMF is also consistent with the radar's monitoring the cusp. Since the latitude of the equatorward boundary of the radar

backscatters and the value of  $D$  from LENA have correlative variations,  $D$  would reflect the motion of the cusp.

It appears that the interval when the radar was receiving the significant backscatter signals roughly corresponds to the interval of high dynamic pressure (shown in Panel (a) of Figure 5). Furthermore, the large enhancement of the dynamic pressure, which is indicated by an arrow in Panel (a), seems to correspond to latitudinally widening the region of the backscattered signals. Presumably, during this large enhancement the soft particle precipitation extended to relatively higher latitudes, and the F-region irregularities produced by the soft particle precipitation occurred in such high latitudes.

Figures 6a and b show the distribution of the LOS flow velocity measured by the Kapuskasing and Goose Bay radars. Figure 6a represents the data obtained at 1552:19 UT, which is the closest timing to the LENA observation shown in Figure 4a, when the time delay of 2.5 min is considered. Figure 6b corresponds to Figure 4b. Figure 6a shows that the equatorward boundary of the cusp backscattered signals occurs at  $\sim 73^\circ$ . The boundary moved equatorward, and reached around  $66^\circ$  at 1604:11 UT (Figure 6b).

## 5. Discussion and Conclusions.

We have shown that the emission observed by LENA in the direction of the high-latitude sheath, the equatorward boundary of the backscattered signals observed by the SuperDARN radars, and the IMF  $B_z$  have correlative variations. This gives evidence to substantiate a means for monitoring the high-altitude cusp using IMAGE/LENA. It should be noted, however, that this correlation is based on the time delay of 20 min between ACE and LENA.

In Figure 1 we estimated the delay time to be 20 min by comparing  $SI^+$  in the geomagnetic index with the solar wind dynamic pressure. Since this time delay includes the propagation time of hydromagnetic waves as  $SI^+$  signals to the Earth from the dayside magnetopause, i.e.,  $\sim 1$  min [e.g., Araki, 1994], the transit time of the solar wind to the dayside magnetopause should be 19 min more or less. In fact, the GOES 8 data indicates that the magnetic field starts to increase about 1 min before the time for the start of the  $SI^+$  on the ground [Taguchi et al., 2003]. However, the detection of the neutral particles by LENA would also delay by one minute or so from the actual motion of the cusp indentation, that is, the neutral particles would take one minute or so to travel the distance from the cusp indentation to the spacecraft. When this distance is assumed to be a couple of Earth radii, and the speed of the neutral particles is approximated as being the same the sheath flow speed, such as  $\sim 200$  km/s, the delay time is about 1 min. Hence, the 20 min time delay from the ACE solar wind to the LENA observation appears to be reasonable.

During the period of significant LENA emission, i.e., 1550-1614 UT IMF  $B_y$  was large, negative (1530-1554 UT in Figure 1). The convection near the cusp in the northern

ionosphere would have a duskward component [e.g., Heppner and Maynard, 1987], and a pair of the  $B_Y$ -dependent cusp field-aligned currents would appear [e.g., Taguchi et al., 1993]. The cusp precipitation region would extend somewhat to earlier MLT on the prenoon side [Newell et al., 1989]. As can be seen from the reddish color in Figure 6b, the fast convection region also appears to be wider in the prenoon than in the postnoon. Although either radar did not cover the mid-noon portion of the ionosphere, presumably the convection is fast there, and the fast convection would occur in a wide MLT region extending from the prenoon to the postnoon. It is very interesting to know to which position in such a wide MLT range the high altitude cusp, which is deduced from the emission observed by LENA, is actually mapped.

In conclusion, the correlation among the LENA emission, the SuperDARN radar signal, and the IMF  $B_Z$  provides evidence for a means for monitoring the high-altitude cusp using IMAGE LENA. The latitudes to which the LENA emission is actually mapped in the ionosphere should be examined with a field line model. Why the latitudinal motion of the radar signals for the sharp changes of less negative IMF  $B_Z$  is not poleward but rather “flat” is also an interesting issue. The two remote sensing observations, i.e., IMAGE/LENA and SuperDARN radar would provide promising opportunities to understand the detailed dynamics of the polar cusp extending from the low-altitudes to the high-altitudes.

### **Acknowledgments.**

ACE solar wind data are provided by NASA/NSSDC. The authors thank D. McComas (PI of ACE plasma data), N. Ness (PI of ACE magnetic field data), and R. Gold (PI of ACE EPAM data). We also thank WDC for Geomagnetism, Kyoto, Japan for providing the midlatitude SYM-H index.

## References

- Araki, T. (1994): A physical model of geomagnetic sudden commencement, in *Solar Wind Sources of Magnetospheric Ultra-Low-Frequency Waves*, *Geophys. Mongr. Ser.*, vol.81, edited by Engebretson, K. Takahashi, and M. Scholer, pp.183-200, AGU, Washington, D.C.
- Baker, K. B., and Wing, S. (1989): A new magnetic coordinate system for conjugate studies of high latitude, *J. Geophys. Res.*, **94**, 9139-9143.
- Baker, K. B., et al. (1990): HF radar and DMSP observation of the cusp: Simultaneous HF radar and DMSP observation of the cusp, *Geophys. Res. Lett.*, **17**, 1869-1873.
- Burch, J. L. (1973): Rate of erosion of the dayside magnetic flux based on a quantitative study of the dependence of polar cusp latitude on the interplanetary magnetic field, *Radio Sci.*, **8**, 955-961.
- Chen, S.-H., Boardsen, S. A., Fung, S. F., Green, J. L. , Kessel, R. L., Tan, L. C., Eastman, T. E., and Craven, J. D. (1997): Exterior and interior polar cusps: Observations from Hawkeye, *J. Geophys. Res.*, **102**, 11,335-11,347.
- Collier, M. R., Slavin, J. A., Lepping, R. P., Szabo, A., and Ogilvie, K. (1998): Timing accuracy for the simple planar propagation of magnetic field structures in the solar wind, *Geophys. Res. Lett.*, **25**, 2509-2512.
- Collier, M. R., et al. (2001a): Observations of neutral atoms from the solar wind, *J. Geophys. Res.*, **106**, 24,893-24,906.
- Collier, M. R., et al. (2001b): LENA Observations on March 31, 2001: Magnetosheath Remote Sensing, *Eos. Trans. AGU*, 82(47), Fall Meeting Suppl., Abstract SM41C-05, F1071-F1072.
- Collier, M. R., et al. (2003): Dust in the wind: The dust geometric cross section at 1 AU based on neutral solar wind observations, in *Solar Wind 10, Proceedings of the Tenth International Solar Wind Conference*, M. Velli, R. Bruno and F. Malara (eds.), AIP Conference Proceedings Volume 679, American Institute of Physics, Melville, New York, pp.790-793.
- Farrell, W. M., and Van Allen, J. A. (1990): Observations of the Earth's polar cleft at large radial distances with the Hawkeye 1 magnetometer, *J. Geophys. Res.*, **95**, 20,945-20,958.
- Fok, M.-C., et al. (2003): Global ENA IMAGE simulations, *Space Sci. Rev.*, **109**, 77-103.
- Fuselier, S. A., Frey, H. U., Trattner, K. J., Mende, S. B., and Burch, J. L. (2002): Cusp aurora dependence on interplanetary magnetic field  $B_z$ , *J. Geophys. Res.*, **107** (A7), 10.1029/2001JA900165.
- Greenwald, R. A., Baker, K. B., Ruohoniemi, J. M., Dudeney, J. R., Pinnock, M., Mattin, N., Leonard, J. M., and Lepping, R. P. (1990): Simultaneous conjugate observations of

- dynamic variations in high-latitude dayside convection due to changes in IMF  $B_y$ , *J. Geophys. Res.*, **95**, 8057-8072.
- Greenwald, R. A., et al. (1995): DARN/SuperDARN: A global view of the dynamics of high-latitude convection, *Space Sci. Rev.*, **71**, 761-706.
- Heppner, J. P., and Maynard, N. C. (1987): Empirical high-latitude electric field models, *J. Geophys. Res.*, **92**, 4467-4489.
- Hosokawa, K., Woodfield, E. E., Lester, M., Milan, S. E., Sato, N., Yukimatu, A. S., and Iyemori, T. (2002): Statistical characteristics of Doppler spectral width as observed by the conjugate SuperDARN radars, *Ann. Geophysicae*, **20**, 1213-1223.
- Iyemori, T., and Rao, D. R. K. (1996): Decay of the Dst component of geomagnetic disturbance after substorm onset and its implication to storm substorm relation, *Ann. Geophysicae*, **14**, 608-618.
- Khan, H., and Cowley, S. W. H. (1999): Observations of the response time of high-latitude ionospheric convection to variations in the interplanetary magnetic field using EISCAT and IMP-8 data, *Ann. Geophysicae*, **17**, 1306-1335.
- Meng, C.-I. (1983): Case studies of the storm time variations of the polar cusp, *J. Geophys. Res.*, **88**, 137-149.
- Milan, S. E., Yeoman, T. K., and Lester, M. (1998): The dayside auroral zone as a hard target for coherent HF radars, *Geophys. Res. Lett.*, **25**, 3717-3720.
- Milan, S. E., Lester, M., Cowley, S. W. H., and Brittnacher, M. (2000): Dayside convection and auroral morphology during an interval of northward interplanetary magnetic field, *Ann. Geophysicae*, **18**, 436-444.
- Moore, T. E., et al. (2000): The low-energy neutral atom imager for IMAGE, *Space Sci. Rev.*, **91** (1-2), 155-195.
- Moore, T. E., et al. (2001): Low energy neutral atoms in the magnetosphere, *Geophys. Res. Lett.*, **28**, 1143-1146.
- Moore, T. E., M. R. Collier, M.-C. Fok, S. A. Fuselier, H. Khan, W. Lennartsson, D. G. Simpson, G. R. Wilson, M. O. Chandler (2003): Heliosphere-Geosphere Interactions Using Low Energy Neutral Atom Imaging, *Space Sci. Rev.*, **109**, 351-371.
- Newell, P. T., and Meng, C.-I. (1988): The cusp and cleft/boundary: Low altitude identification and statistical local time variations, *J. Geophys. Res.*, **93**, 14,549-14,556.
- Newell, P. T., Meng, C.-I., Sibeck, D. G., and Lepping, R. P. (1989): Some low-altitude cusp dependencies on interplanetary magnetic field, *J. Geophys. Res.*, **94**, 8921-8927.
- Pinnock, M., Roger, A. S., Dudeney, J. R., Baker, K. B., Greenwald, R. A., and Greenspan, M. (1993): Observations of an enhanced convection channel in the cusp ionosphere, *J. Geophys. Res.*, **98**, 3767-3776.
- Ruohoniemi, J. M., Greenwald, R. A., de la Beaujardiere, O., and Lester, M. (1993): The response of the high-latitude dayside ionosphere to an abrupt northward transition in the IMF, *Ann. Geophysicae*, **11**, 544-555.

- Sandholt, P. E. et al. (1994): Cusp/cleft auroral activity in relation to solar wind dynamic pressure, interplanetary magnetic field  $B_z$  and  $B_y$ , *J. Geophys. Res.*, **99**, 17,323-17,342.
- Sandholt, P. E., Farrugia, C. J., Oieroset, M., Stauning, O., and Denig, W. F. (1998): Auroral activity associated with unsteady magnetospheric erosion: Observations on December 18, 1990, *J. Geophys. Res.*, **103**, 2309-2317.
- Taguchi, S., Sugiura, M., Winningham, J. D., and Slavin, J. A. (1993): Characterization of the IMF  $B_y$ -dependent field-aligned currents in the cleft region based on DE 2 observations, *J. Geophys. Res.*, **98**, 1393-1407.
- Taguchi, S., Collier, M. R., Moore, T. E., Fok, M.-C., and Singer, H. J. (2003): Response of neutral atom emissions in the low- and high-latitude magnetosheath direction to the magnetopause motion under extreme solar wind conditions, *J. Geophys. Res.*, in press.
- Yeoman, T. K., Lester, M., Cowley, S. W. H., Milan, S. E., Moen, J., and Sandholdt, P. E. (1997): Simultaneous observation of the cusp in optical, DMSP, and HF radar data, *Geophys. Res. Lett.*, **24**, 2251-2254.
- Zhou, X. W., Russell, C. T., Le, G., Fuselier, S. A., and Scudder, J. D. (2000): Solar wind control of the polar cusp at high altitude, *J. Geophys. Res.*, **105**, 245-251.

## Figure Captions

**Figure 1.** ACE Solar wind data, and SYM-H for the event in this study. (a) Flux of energetic ions with energies between 47 and 65 keV/e (in unit of counts  $\text{s}^{-1}\text{cm}^{-2}\text{ster}^{-1}\text{MeV}^{-1}$ ), (b) IMF  $B_Y$ , (c) IMF  $B_Z$ , (d) solar wind number density, (e) GSM  $X$  component of velocity, (f) RAM pressure, and (g) the H-component of the SYM index. The vertical lines in (g) represent the times for the start of  $\text{SI}^+$ , and the times for the corresponding ACE RAM pressure jump, which is identified in (f), are shown with the vertical lines in the ACE plasma data.

**Figure 2.** Position of IMAGE in GSM  $X$ - $Z$  plane for 1540 – 1620 UT April 11, 2001.

**Figure 3.** Variations of (a) the IMAGE position, (b) the LENA spin angle, (c) the hydrogen total count rates, (d) the normalized counts in each time and range bin, and (e) the distance representing the direction for the maximum count peaks during a period of the significant emission. The inset of (e) illustrates the definition of the distance  $D$ , which is plotted in this panel.

**Figure 4.** LENA image obtained around (a) 1549:20 UT, and (b) 1601:47 UT April 11, 2001. Background adjusted hydrogen count rates are plotted in the format of the spin angle versus the polar angle.

**Figure 5.** Variations of (a) ACE dynamic pressure, (b) IMF  $Z$ -component, and (c) flow velocity of the ionospheric convection obtained with the SuperDARN radar (Beam 5) at Goose Bay, and the distance representing the direction of the high-latitude peak emission observed by LENA (black rectangle). The ACE data are delayed by 20 min, and the radar data are forwarded by 2.5 min. These data are superimposed in an arbitrary scale along the vertical axis.

**Figure 6.** Distribution of the velocity of the convection obtained at Goose Bay (indicated with G) and Kapuskasing (shown with K) SuperDARN radars (a) at 1552:19 UT and (b) at 1604:11 UT.

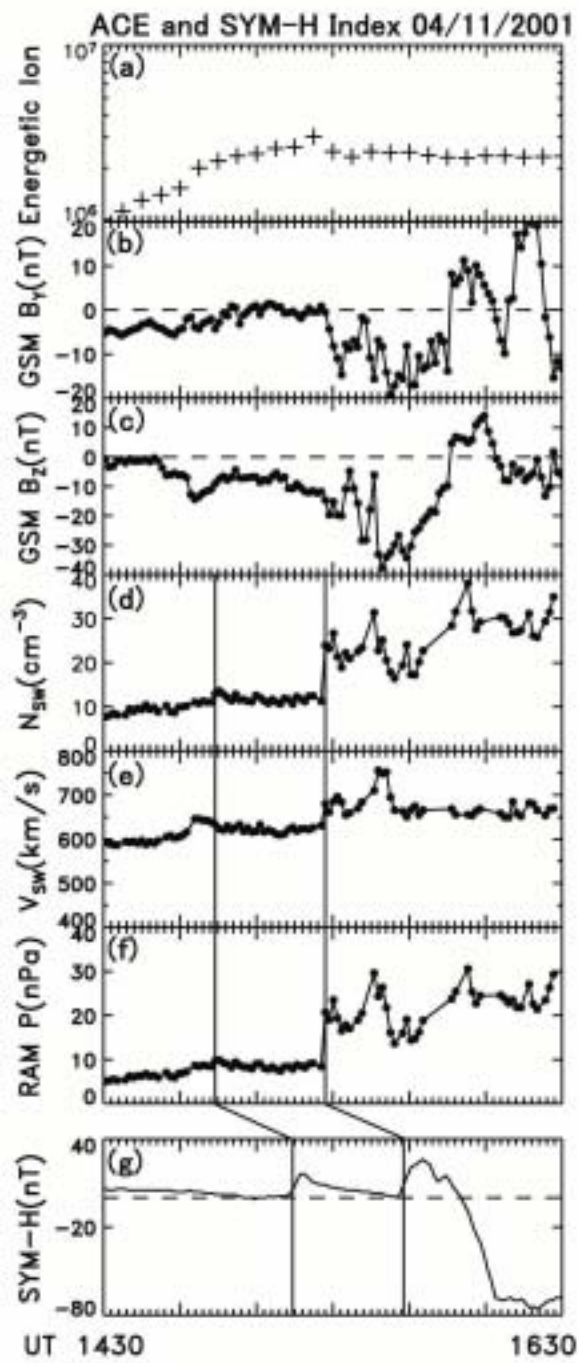


Figure 1. Taguchi et al.

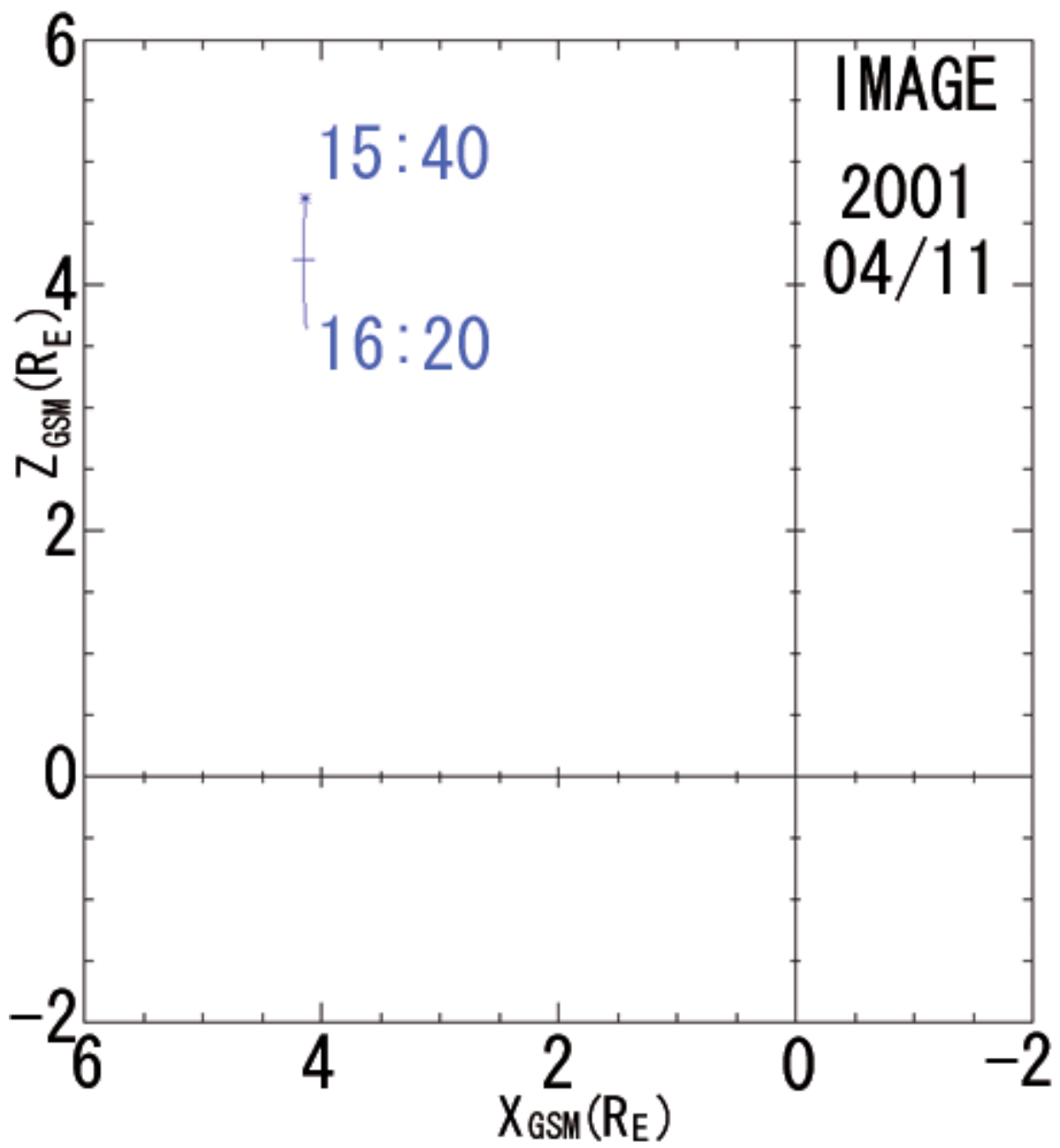


Figure 2. Taguchi et al.

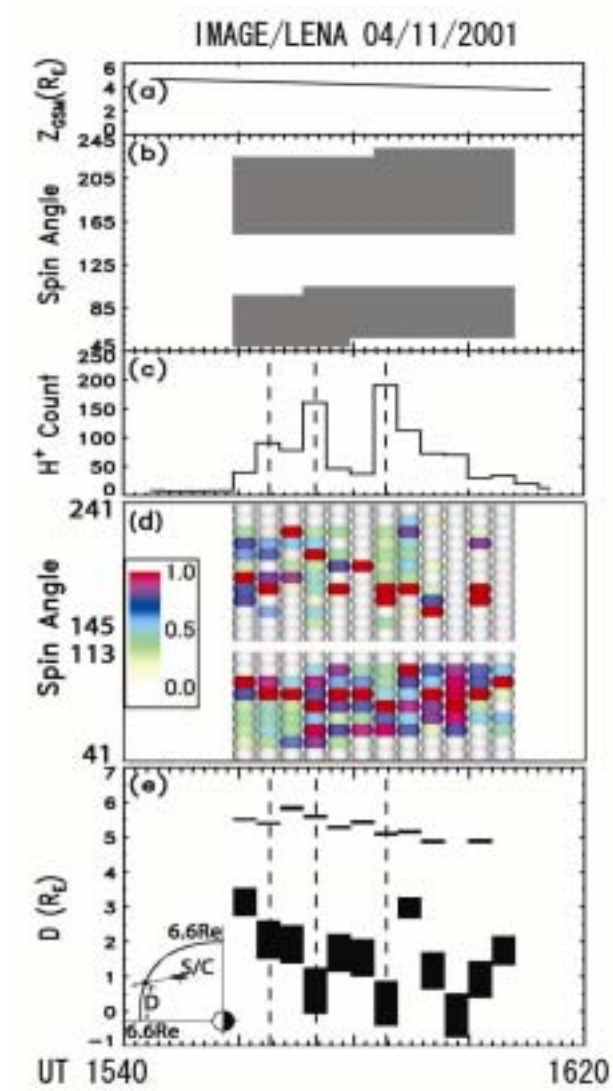
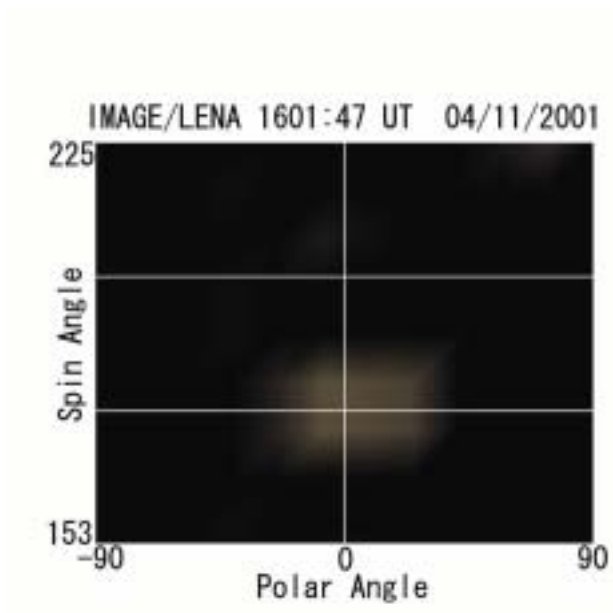
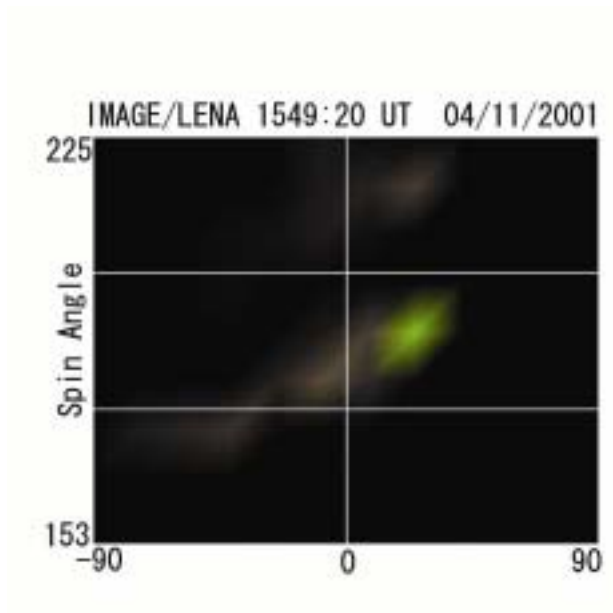


Figure 3. Taguchi et al.



Figures 4a and 4b. Taguchi et al.

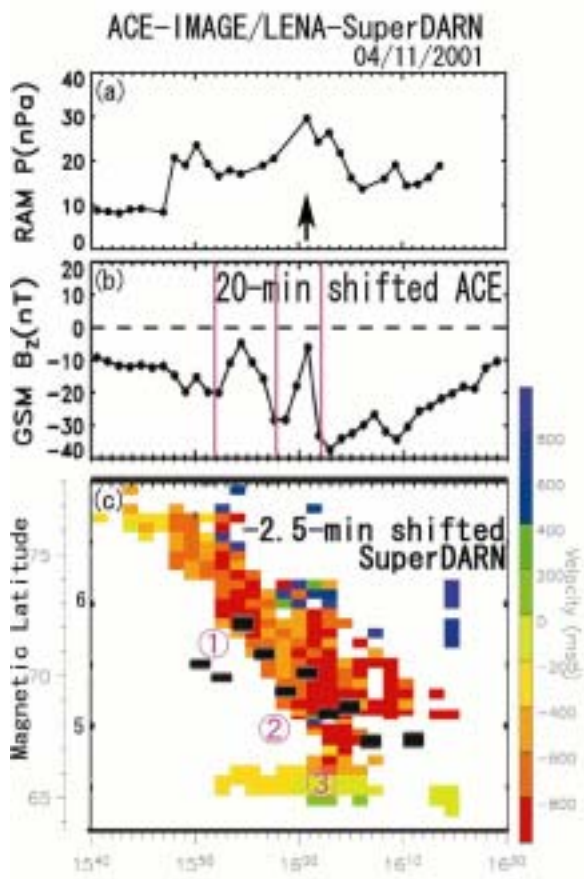


Figure 5. Taguchi et al.

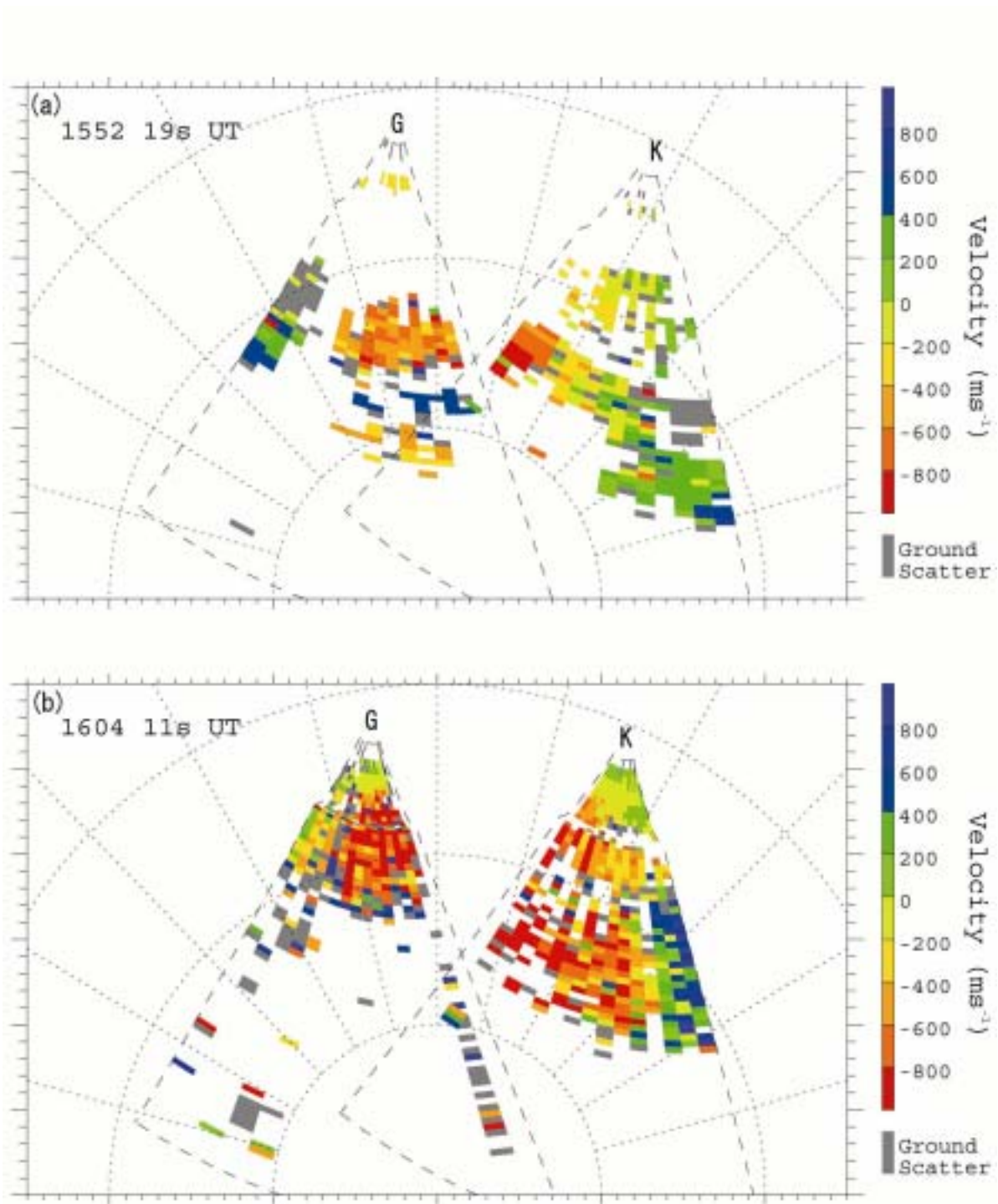


Figure 6. Taguchi et al.